

Input Coupling and Guided-wave Distribution Schemes for Board-level Intra-chip Guided-Wave Optical Clock Distribution Network Using Volume Grating Coupler Technology¹

Anthony V. Mule¹ *Student Member, IEEE*, Stephen M. Schultz², Elias N. Glytsis, *Senior Member, IEEE*, Thomas K. Gaylord, *Fellow, IEEE*, and James D. Meindl, *Life Fellow, IEEE*
 Microelectronics Research Center, Georgia Institute of Technology, Atlanta, GA 30332
 (Email: gt2925a@prism.gatech.edu)

Abstract

The input coupling and guided-wave distribution schemes for a novel board-level guided wave optical clock distribution network using volume grating coupler technology are described. Volume grating coupler technology is employed to couple light into the optical waveguide distribution with high efficiency, allowing for compact packaging of the entire optical system and reduced optical input power requirements. A novel single-split-region waveguide distribution network is proposed to allow for larger radii of curvature in the final, smallest-radii levels for reduced bending loss in comparison to a conventional multiple-split-region topology.

Introduction

Performance limitations imposed by global clock interconnect, in addition to short-term jitter induced within distributed clock buffers and clock multipliers, impose the most stringent limitations on system-level performance as local clock frequencies of high performance microprocessors progress into the multi-GHz regime. Figure 1 illustrates a plot of 3 dB interconnect bandwidth vs. length for global interconnect corresponding to the sixth metal level of a 0.18 μm copper interconnect technology process. As Figure 1 illustrates, the maximum length of global interconnect allowed for a specific bandwidth decreases with increasing interconnect length. This implies the need for an increasing number of global clock repeaters along a significant length of global clock interconnect to compensate for insufficient bandwidth. An increase in the number of clock repeaters in turn increases cycle-to-cycle jitter contained within the signal due to dynamic variations in the power supply. This trend is reflected in Figure 2 where the percentage of test period consumed by cycle-to-cycle jitter of the PLL/global distribution network of several high performance microprocessors is plotted vs. test frequency. The use of simple local clock multipliers to multiply lower-frequency global clock signals to higher-frequency local clock signals [1] results in the amplification of any jitter at the multiplier input [2]. As such, the design of global clock interconnect in GHz clock distribution networks is subject to a *bandwidth-jitter tradeoff* with respect to performance. This tradeoff represents a primary motivation for investigating optical methods of global clock distribution in GHz microprocessors.

¹This work is supported by the Semiconductor Research Corporation (Contract: SJ-374)

²The author is with Raytheon Missile Systems, Tucson, AZ

Proposed Inter-chip/Intra-chip Optical Clock Distribution Network

A novel board-level guided wave optical clock distribution network using high-efficiency volume grating coupler technology has been proposed in [3] for achieving global propagation of the local clock frequency in an intra-board/inter-chip and intra-chip fashion. The focus of this analysis is with respect to the input coupling and guided-wave portion of the distribution network. The proposed system exhibits the following key features: a) no on-chip photonic sources; b) monolithic silicon-based detection; c) global optical signal propagation through a board-level guided-wave H-tree distribution; and d) the use of volume grating coupler technology to redirect light into and out of the board-level distribution. Guided-wave propagation employing volume grating coupler technology allows for compact planar packaging of the optical/electrical system, a reduction in the required optical input power due to the high efficiency of the input and output coupling elements, and a reduction in the chip-level detector area required for complete coverage of the optical beam under wavelength and spatial variations through the use of a volume focusing grating output coupler.

Volume Non-focusing Grating Input Coupler

The proposed optical input to the guided wave distribution is a board-level vertical cavity surface emitting laser (VCSEL) source driven by a dedicated CMOS circuit, where the optical output is collimated through a micro-lens array for coupling into a volume non-focusing grating input coupler. A top-down schematic of the volume non-focusing grating input coupler is depicted in Figure 3. Through the theory of reciprocity, the input coupling efficiency of a volume non-focusing grating coupler, η_{input} , can be approximated by the overlap integral of an arbitrary input field with the output field produced by the grating input coupler. The total power coupled out of a volume non-focusing grating input coupler is given by

$$P_{\text{out}} = P_o \left[1 - \exp(-2\alpha_{\text{input}} L_{\text{input}}) \right] \quad (1)$$

In Eq. (1), L_{input} is the length of the input coupler, and α_{input} is the coupling coefficient. The output power is divided between the orders present at the output, where the preferential coupling efficiency into the desired order is represented by η_{pref} . The intensity of the out-coupled power at the surface of the grating is given by

$$I_{\text{out}} = P_o \eta_{\text{pref}} \left[1 - \exp(-2\alpha_{\text{input}} L_{\text{input}}) \right] 2\alpha_{\text{input}} \exp(-2\alpha_{\text{input}} x) \quad (2)$$

where P_0 is the power initially guided within the waveguide, and x represents the longitudinal position along the length of the coupler. The input optical beam is taken to stem from a collimated source, resulting in a beam with a uniform input intensity of $I_{in} = P_0/L_{input}$. To determine the overlap of the field profiles, the total (normalized) power in each of the reciprocal cases is set equal to 1. Under conservation of normalized power, the input coupling efficiency is given by

$$\eta_{input} = \int_0^{L_{input}} \sqrt{I_{out} \cdot I_{in}} dx \quad (3)$$

Substituting Eq. (2) into Eq. (3) and setting $P_0 = 1$, the input coupling efficiency is given by

$$\eta_{input} = \left(P_0 \eta_{pref} [1 - \exp(-2\alpha_{input} L_{input})] \right)^{1/2} \frac{1}{\alpha_{input}} [1 - e^{-\alpha_{input} L_{input}}] \quad (4)$$

Assuming a preferential coupling efficiency of $\eta_{pref} = 0.98$ [4-7], a maximum input coupling efficiency of 86.5 % is predicted for an input coupler with $\alpha_{input} = 0.0015 \mu\text{m}^{-1}$ and $L_{input} = 1 \text{ mm}$.

Equation (4) assumes exact phase matching between the input and output beams. This implies the incident angle of the input beam is the same as the angle of the output beam. As the angle of the out-coupled beam is dependent on the optical wavelength, a variation in wavelength produces a phase mismatch for a fixed input beam angle of incidence. A vertical misalignment of the source with respect to the coupler will have a negligible effect due to the collimation of the source. A lateral misalignment will also produce a negligible effect as long as the beam remains within the area encompassed by the grating. The lateral width of the grating can be increased to account for lateral deviations. A longitudinal shift of the source with respect to the coupler results in a change in the overlap integral and thus a reduction in input coupling efficiency. Figure 4 illustrates the reduction in input coupling efficiency as a function of longitudinal displacement. For longitudinal shifts of + 25 μm and - 25 μm , the input coupling efficiency reduces by 1.0 % and 3.2 %, respectively.

Single-split-region Waveguide Distribution

Following the distribution input is a single-mode waveguide which feeds both the inter-chip and subsequent intra-chip distribution(s). With respect to the intra-chip distribution, splitting of the optical power between respective distribution arms is achieved using multi-mode interference (MMI) power splitters. MMI power splitters offer reduced optical loss, reduced device dimensions, and compatibility with high refractive index contrast waveguiding [8]. A key property of MMI power splitters is the ability to split the input optical power into a number of fanout arms ≥ 2 .

This increased fanout allows for the splitting of optical input power within a single region prior to the fanout portion of the distribution. A single-split-region distribution topology that takes advantage of the greater degree of fanout to allow for near-maximum radii of propagation in the final, smaller radii levels is illustrated in Figure 5 for a fanout of 16.

Potential choices for the single-split-region architecture are illustrated in Figure 5b. To estimate the minimum spacing required between parallel waveguides for negligible waveguide-to-waveguide crosstalk within the distribution, a plot of the coupling coefficient κ_i vs. edge-to-edge separation distance d_{wg} between waveguides is generated using three-dimensional Beam Propagation Method (BPM) software assuming the rib waveguide of Figure 6. The single guided mode intensity diagram is shown in Figure 6b. For an optical wavelength $\lambda_0 = 0.85 \mu\text{m}$ and waveguide dimensions $t_{buff} = 10 \mu\text{m}$, $t_{wg} = 0.5 \mu\text{m}$, $t_{rib} = 0.5 \mu\text{m}$, $w_{wg} = 2 \mu\text{m}$, $n_{core} = 1.54$, $n_{clad} = 1$, and $n_{sub} = 1.51$, BPM crosstalk simulations illustrated in Figure 7 result in a minimum allowable spacing $d_{wg} = 4.5 \mu\text{m}$ for the buried channel waveguide geometry. For this spacing, the waveguide-to-waveguide crosstalk is negligible. Given d_{wg} , w_{wg} , and the target chip area, the radii of curvature inherent to a single-split-region distribution can be obtained. Table 1 lists the ideal and minimum radii of propagation corresponding to the i^{th} arc of the k^{th} level, where $k = \{1 \dots m\}$, m is the total number of H's encountered per path, and $i = \{1, 2\}$ for the first and second arc of each level, respectively. The global skew inherent to a single-split-region distribution as a function of fanout is illustrated in Figure 8. Global skew due to unequal path lengths within a single-split-region distribution is $\leq 9 \text{ ps}$ for a fanout of 256 and a die area of 817 mm^2 . This component of global skew represents a fixed, predictable value in contrast to the variable skew inherent to global electrical clock distribution networks.

Conclusions

A large-area volume non-focusing grating input coupler for coupling light into a board-level inter-chip/intra-chip optical waveguide clock distribution network is presented. Assuming collimation of the optical source, a input coupling efficiency of 83.3 % is predicted under worst-case placement variations. A single-split-region H-tree topology is proposed for the intra-chip portion of the distribution network to allow for near-ideal radii of curvature in the final, smallest radii levels. A maximum global skew of 9 ps is found for a single-split distribution achieving a fanout of 256.

References

1. 1999 SIA International Technology Roadmap for Semiconductors (ITRS).
2. B. Razavi, *RF Microelectronics*. New Jersey: Prentice Hall, 1998.
3. A. Mule', S. Schultz, T. K. Gaylord, and J. D. Meindl, *Proc. IEEE International Interconnect Technology Conference*. San Francisco, CA: pp. 6-8, June 2000.
4. S. M. Schultz, E. N. Glytsis, and T. K. Gaylord, *Applied Opt.*, vol. 37, pp. 2278-87, April 1998.
5. S. M. Schultz, E. N. Glytsis, and T. K. Gaylord, *Opt. Lett.*, vol.24, pp. 1-3, Dec. 1999.
6. S. M. Schultz, E. N. Glytsis, and T. K. Gaylord, *Applied Opt.*, vol. 39, pp.1223-1232, Mar. 2000.
7. S. M. Schultz, E. N. Glytsis, and T. K. Gaylord, "Diffractive grating coupler and method," U. S. patent application, Oct. 2, 1998.
8. L. B. Soldano and E. C. M. Pennings, *J. Lightwave Technol.*, vol. 13, pp. 615-627, Apr. 1995.

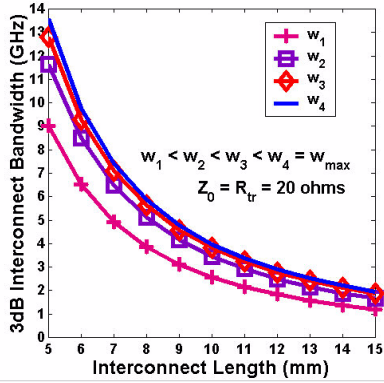


Figure 1: 3 dB bandwidth of global GSI clock interconnect (GHz) vs. length for increasing width (proprietary technology).

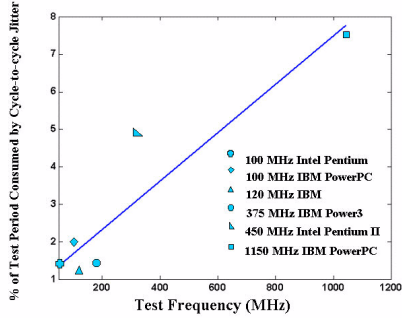


Figure 2: Percentage of test period consumed by cycle-to-cycle jitter vs. test frequency for aggregate global clock distribution network (PLL + global buffers, interconnection) of given microprocessors.

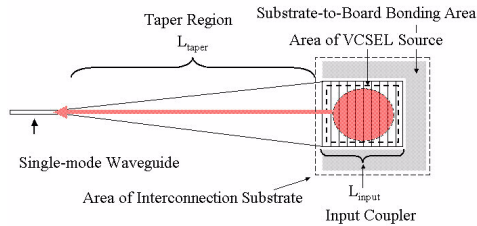


Figure 3: Top-down view of volume non-focusing grating input coupler.

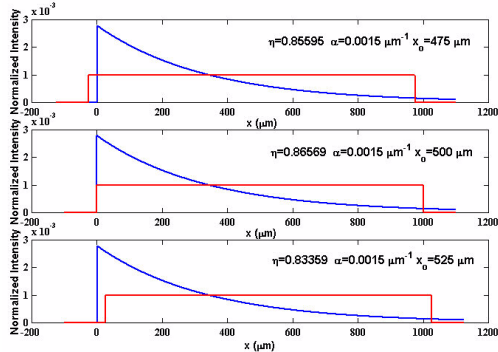


Figure 4: Plot of normalized intensity vs. location along coupler for longitudinal shift of optical source of a) -25 μm, b) 0 μm (ideal), and c) +25 μm

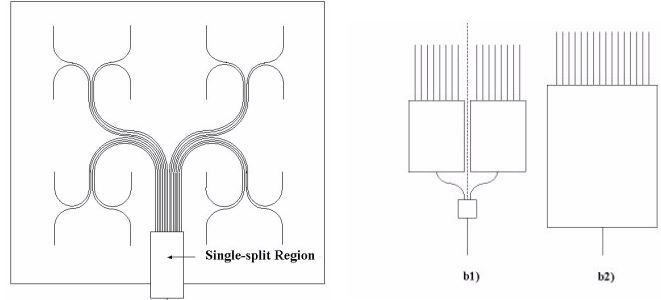


Figure 5: a) Novel single-split-region H-tree distribution for fanout of 16 and b) potential single-split-region architectures.



Figure 6: a) Rib waveguide geometry and b) field profile.

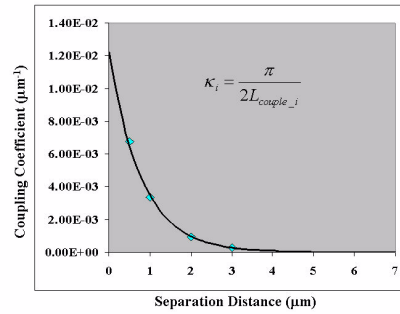


Figure 7: Coupling coefficient κ vs. waveguide spacing d_{wg} .

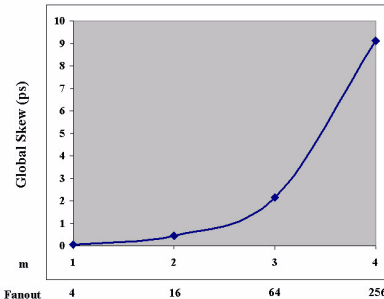


Figure 8: Global skew of concentrated split distribution vs. fanout.

Table 1: Radii of curvature for single-split-region topology

k	i	Ideal Radius	Minimum Radius	% Difference
1	1	3572.90	2744.15	23.20
1	2	3572.90	3160.15	11.55
2	1	1786.45	1581.70	11.46
2	2	1786.45	1685.70	5.64
3	1	893.23	844.48	5.46
3	2	893.23	870.48	2.55
4	1	446.61	436.86	2.18
4	2	446.61	443.36	0.73

